11th World Congress on Computational Mechanics (WCCM XI)
5th European Conference on Computational Mechanics (ECCM V)
6th European Conference on Computational Fluid Dynamics (ECFD VI)
July 20–25, 2014, Barcelona, Spain

TRANSONIC COMBUSTION: STEADY AND UNSTEADY POTENTIAL MODELS

William E. Tavernetti[1] and Mohamed M. Hafez[2]

[1] Graduate Student, Department of Mathematics, University of California, One Shields Ave. Davis, CA 95616, etavernetti@math.ucdavis.edu
[2] Professor, Department of Mechanical Engineering, University of California, One Shields Ave. Davis, CA 95616, mhafez@ucdavis.edu

Key words: *Transonic, Combustion, TSD, Small Disturbance, Inviscid, Compressible, Premixed, Arrhenius, Full Potential*

Theoretical studies of combustion have mostly focused on low speed deflagrations as well as pure supersonic detonations; however, transonic conditions, have not been as widely studied. Transonic flow conditions naturally occur in a variety of applications such as: turbine engines, power generation systems, missiles, turbo-machinery, industrial reactors and many more. Transonic flows are particularly sensitive to changes in geometry and other conditions of the flow, and understanding these effects can be important for avoiding large performance degradation for flows at off design conditions. A small disturbance and irrotational model is proposed in [8]. The current work investigates relaxing the small disturbance assumption. In addition, the common practice is to treat the pressure equation as elliptic (pressure correction methods, pressure projection methods,...). Instead, a hyperbolic equation for the pressure is used in this study for unsteady problems. The current work investigates integration of the hyperbolic pressure equation as part of a reactive full potential flow model.

1 Introduction

Increasingly computer simulations are being used in engineering, and simulations involving the reactive Euler equations are expensive and can reduce the number of calculations a design team can test. For this reason, lower cost models that simplify the problem, such as lower dimensional, small disturbance, or potential models, which may be permissible under certain operating conditions are desirable. The present work has two principal goals: (1) to extend the small disturbance combustion model propsed in [8] for transonic flows, and (2) to develop a pressure-based unsteady full potential model that is capable of handling the effect of chemical reactions. In this work we investigate a natural alternative model that fits between a reactive small disturbance model and a full reactive Euler model.

2 Combustion Modeling

The general governing equations are the two-dimensional compressible reactive flow Equations for a premixed chemical fuel species with Arrehenius type kinetics:

$$\begin{aligned}
\rho_t + (\rho u)_x + (\rho v)_y &= 0 \\
(\rho u)_t + (\rho u^2)_x + (\rho v u)_y + p_x &= \mu\left(u_{xx} + u_{yy} + \frac{1}{3}\left(u_x + v_y\right)_x\right) \\
(\rho v)_t + (\rho u v)_x + (\rho v^2)_y + p_y &= \mu\left(v_{xx} + v_{yy} + \frac{1}{3}\left(u_x + v_y\right)_y\right) \\
(\rho C_p T)_t + \left(\rho u\left[T + \frac{1}{2}\left(u^2+v^2\right)\right]\right)_x + \left(\rho v\left[T + \frac{1}{2}\left(u^2+v^2\right)\right]\right)_y &= \lambda\Delta\left(T + \frac{1}{2}(u^2+v^2)\right) + \Phi_\mu + \Phi_D + Bw \\
(\rho Y)_t + (\rho u Y)_x + (\rho v Y)_y &= D\Delta Y - w \\
p &= \rho R_{gas} T \\
w &= D_a \rho Y e^{-\frac{Ea}{R_{gas}T}}
\end{aligned} \tag{1}$$

Where μ is the viscosity, λ is the thermal conductivity, A is the pre-exponential reaction factor, and D is the diffusivity coefficient, Φ_μ is the viscous dissipation and Φ_D is the mass diffusion. The choice of premixed chemistry with Arrhenius kinetics is to emphasize the effect of heat release with realistic reaction rates coupled to the flow.

2.1 Nondimensionalization

Letting the ∞-state denote the uniform flow conditions at the channel inlet, a non-dimensionalization is made by, where $[\cdot]$ denotes a dimensional variable, ∞ the inlet condition and L is half the width of the channel:

$$\begin{aligned}
M_\infty = \frac{u_\infty^2}{\gamma R_{gas} T_\infty}, \quad \rho = \frac{[\rho]}{\rho_\infty}, \quad p = \frac{[p]}{\rho_\infty u_\infty^2} = \frac{[p]}{p_\infty \gamma M_\infty^2}, \\
T = \frac{[T]}{(V_\infty^2/C_p)}, \quad u = \frac{[u]}{u_\infty}, \quad v = \frac{[v]}{v_\infty}, \quad Y = \frac{Y}{\|Y\|_\infty} \quad x = \frac{[x]}{L}, \quad y = \frac{[y]}{L}
\end{aligned} \tag{2}$$

Y is a reaction progress variable, $0 \leq Y \leq 1$, where $Y = 0$ means the reactant is fully consumed, and $Y = 1$ implies no reaction has yet taken place. Some authors non-dimensionalize $T = \frac{[T]}{T_\infty}$, a conversion between this non-dimensionalization and ours is given by:

$$T = \frac{[T]}{(V_\infty^2/C_p)} = \frac{[T]}{T_\infty}\frac{1}{\gamma - 1}\frac{1}{M_\infty^2} \tag{3}$$

The dimensionless parameters are given by:

$$M_\infty^2 = \frac{u_\infty^2}{\gamma R_{gas} T_\infty}, \quad A = \frac{D_a}{u_\infty}, \quad \theta = \frac{Ea}{C_p T_\infty}\frac{1}{\gamma - 1}\frac{1}{M_\infty^2}, \quad \beta = \frac{[B]}{u_\infty^2} = \frac{[B]}{C_p T_\infty}\frac{1}{\gamma - 1}\frac{1}{M_\infty^2}, \tag{4}$$

Now, the dimensionless governing equations, in the inviscid limit of the momentum equations, without viscous dissipation or mass diffusion become:

$$\begin{gathered}
\rho_t + (\rho u)_x + (\rho v)_y = 0, \quad f := (\rho u)_t + (\rho u^2)_x + (\rho v u)_y = -p_x, \quad g := (\rho v)_t + (\rho u v)_x + (\rho v^2)_y = -p_y \\
(\rho T)_t + \left(\rho u \left[T + \frac{1}{2}\left(u^2 + v^2\right)\right]\right)_x + \left(\rho v \left[T + \frac{1}{2}\left(u^2 + v^2\right)\right]\right)_y = \frac{1}{Pr \cdot Re}\Delta\left(T + \frac{1}{2}(u^2 + v^2)\right) + \beta w \\
(\rho Y)_t + (\rho u Y)_x + (\rho v Y)_y = \frac{1}{Sc \cdot Re}\left(Y_{xx} + Y_{yy}\right) - w \\
p = \rho T \frac{\gamma - 1}{\gamma} \\
w = A \rho Y e^{-\frac{\theta}{T}}
\end{gathered} \tag{5}$$

This is a model for the reactive Euler Equations for compressible flow with premixed Arrhenius combustion.

3 Reactive Transonic Full Potential Model

Decomposition of the velocity field into a curl-free component and a divergence-free component gives:

$$u = \phi_x + \frac{\psi_y}{\rho}, \qquad v = \phi_y - \frac{\psi_x}{\rho}, \tag{6}$$

This Helmholtz orthogonal decomposition of the velocity field gives us a non-dimensional pressure based potential and stream function formulation for the compressible Euler equations (5) without combustion (A = 0):

$$\begin{gathered}
(\rho\phi_x)_x + (\rho\phi_y)_y + \rho_t = 0, \quad \left(\frac{\psi_x}{\rho}\right)_x + \left(\frac{\psi_y}{\rho}\right)_y = -\omega \\
(\rho u \omega)_x + (\rho v \omega)_y = F(\rho, \omega), \qquad f_x + g_y = \rho_{tt} - (p_{xx} + p_{yy}) \\
\rho T_t + \rho u \left[T + \frac{1}{2}\left(u^2 + v^2\right)\right]_x + \rho v \left[T + \frac{1}{2}\left(u^2 + v^2\right)\right]_y = \frac{1}{Pr \cdot Re}\Delta\left(T + \frac{1}{2}(u^2 + v^2)\right)
\end{gathered} \tag{7}$$

Where f and g stand for the inertia terms in the momentum equations. The above Poisson equation for the pressure is derived by taking the divergence of the momentum equations in primitive variables:

$$-\nabla \cdot \nabla p = \frac{\partial f}{\partial x} + \frac{\partial g}{\partial y} = \nabla \cdot \vec{F} + \frac{\partial \nabla \cdot \rho u}{\partial t} = \nabla \cdot \vec{F} + \frac{\partial^2 \rho}{\partial t^2} \tag{8}$$

This model admits the incompressible flow solution as a special case when density is constant. Some simplifications of the above model are possible. For example, in the case of irrotational compressible flow, the stream function equation can be omitted, and in the case of irrotational incompressible flow, instead of the pressure equation, Bernoulli's law can be used. We will assume the flow is irrotational (i.e. $\omega = \nabla \times \vec{V} = 0$), but we will account for heat release due to chemical reaction coupling as in the reactive Euler

Equations. In particular, for the expanding duct flow under consideration in this paper, shock fronts are almost normal to the principal flow direction. Since Crocco relation relates vorticity to shock curvature, this suggests a framework where under such conditions a compressible potential flow model might be used.

For irrotational flows, a velocity potential function ϕ must exist such that $\vec{q} = \nabla\phi$. Under this assumption the velocity field is curl-free and reduces to: $u = \phi_x$, $v = \phi_y$. An irrotational unsteady compressible reactive full potential flow model is given by:

$$\begin{aligned}
(\rho\phi_x)_x + (\rho\phi_y)_y + \rho_t &= 0 \\
\left[(\rho u^2)_x + (\rho uv)_y\right]_x + \left[(\rho uv)_x + (\rho v^2)_y\right]_y - \frac{1}{Pr\cdot Re}\Delta\left((\rho u)_x + (\rho v)_y\right) &= \rho_{tt} - (p_{xx} + p_{yy}) \\
\rho T_t + \rho u\left[T + \frac{1}{2}\left(u^2+v^2\right)\right]_x + \rho v\left[T + \frac{1}{2}\left(u^2+v^2\right)\right]_y &= \frac{1}{Pr\cdot Re}\Delta\left(T + \frac{1}{2}(u^2+v^2)\right) + \beta w \\
\rho Y_t + \rho u Y_x + \rho v Y_y &= \frac{1}{Sc\cdot Re}\left(Y_{xx} + Y_{yy}\right) - w \\
p &= \rho T\frac{\gamma-1}{\gamma} \\
w &= A\rho Y e^{-\frac{\theta}{T}}
\end{aligned} \tag{9}$$

It should be noted that unlike the classical density-based approach, this is a pressure-based approach. For steady flow, the pressure equation can be treated as a Poisson's equation. For unsteady flow, the following hyperbolic equation for pressure introduced:

$$\rho_{tt} = (p_{xx} + p_{yy}) + f_x + g_y \longrightarrow \frac{\gamma}{\gamma-1}\left(\frac{p}{T}\right)_{tt} = (p_{xx} + p_{yy}) + f_x + g_y \tag{10}$$

In these simulations the diffusive terms act more as a stabilizing artificial viscosity rather than being representative of physical terms as in the temperature and species equations. Although, for the temperature and species equations, our intention here is not to match a particular experimental fluid with the choice of Re, Pr, Sc. For this reason we simply choose:

$$\frac{1}{Sc\cdot Re} = \frac{1}{Pr\cdot Re} = O(\Delta x) \tag{11}$$

4 Reactive Transonic Small Disturbance Model

Using a small disturbance expansion around a uniform steady state (V_∞=1) gives a reactive transonic small disturbance model similar to that proposed in [8]:

$$\begin{aligned}
\left[1 - M_\infty^2 - (\gamma+1)M_\infty^2\varphi_x\right]\frac{\partial^2\varphi}{\partial x^2} + \frac{\partial^2\varphi}{\partial y^2} &= \tilde{\beta}K_\delta\tilde{A}\tilde{Y}e^{-\tilde{\theta}/(1+\tilde{T})} \\
\tilde{T} = -(\gamma-1)\varphi_x, \quad \tilde{Y}_x &= \tilde{A}\tilde{Y}e^{-\tilde{\theta}/(1+\tilde{T})}
\end{aligned} \tag{12}$$

This governing equation is of mixed type, elliptic and hyperbolic. Here $\tilde{T}, \tilde{Y}$ denotes small disturbance variables, and $\tilde{A},\ \tilde{\beta},\ K_{\tilde{V}}$, and $\tilde{\theta}$ are constant reaction control parameters. The velocity can be calculated from: $\tilde{u} = \varphi_x,\ \ \tilde{v} = \varphi_y$. Details of the derivation, scaling, and variations are available in [8]. The small disturbance approach is limited to small heat release, i.e. diluted premixtures, and small area variation. According to [8] the precise limitations are upstream flows with Mach number between 0.75 and 1.2, premixtures with reactant mass fractions up to 0.1, and channel cross-sectional area variation of 15 percent or less. The boundary conditions at the channel inlet ($-1 \leq y \leq 1$) are:

$$u(0,y) = 1 + \alpha u_0(y),\ v_x(0,y) = 0,\ T(0,y) = 1 + \alpha T_0(y),\ Y(0,y) = \delta Y_0(y) \tag{13}$$

where $0 \leq \alpha << 1$. We will take $\alpha = 0$ in these calculations. At the channel outlet ($y_{lower} \leq y \leq y_{upper}$),:

$$v(x_{out}, y) = 0,\ \frac{\partial T(x_{out}, y)}{\partial y} = 0,\ \frac{\partial Y(x_{out}, y)}{\partial y} = 0 \tag{14}$$

Along the channel walls:

$$v \approx \frac{dG_{body}}{dx} \tag{15}$$

As in [**?**] the nozzle geometry divergence is specified smoothly from a cosine continuation at $x = 1$:

$$G_{body}(x) = \begin{cases} 1, & \text{for } x < 1 \\ \frac{1}{2}\left[2 + \epsilon_{wall}\left(1 + \cos\left(\pi x\right)\right)\right], & \text{for } 1 \leq x \leq 2 \\ 1 + \epsilon_{wall}, & \text{for } 2 < x \leq 3 \end{cases} \tag{16}$$

Typically $\epsilon_{wall} = 0.12 = 12\%$, unless otherwise specified, as in Figure 3. We assume a symmetric flow, at the axis of symmetry, where $y = 0$:

$$v(x,0) = 0,\ T_y(x,0) = 0,\ Y_y(x,0) = 0 \tag{17}$$

In these calculations: $\tilde{\beta}K_\delta = 2,\ \tilde{\theta} = 12, \tilde{A} = \epsilon^{2/3}A$. The mesh is 181 points in the x-direction from $x = 0$ to $x = 3$, and 101 points in the y-direction from $y = 0$ to $y = 1$. In this case, the 4-point operator of Murman-Cole is used to solve this mixed type elliptic hyperbolic equation with line successive under relaxation implicit in the y-direction [6]. The reaction ODE is solved with Simpson's integration method as in [8]. The Mach number is calculated by:

$$M_a = M_\infty \sqrt{(1 + (\gamma + 1)\tilde{u})} \tag{18}$$

Non-reactive and reactive validation test cases are shown below and are in good agreement with [8]. Example results showing the transition from fully subsonic to shocked flow with a supersonic bubble for the non-reactive flow are given in Figure 1.

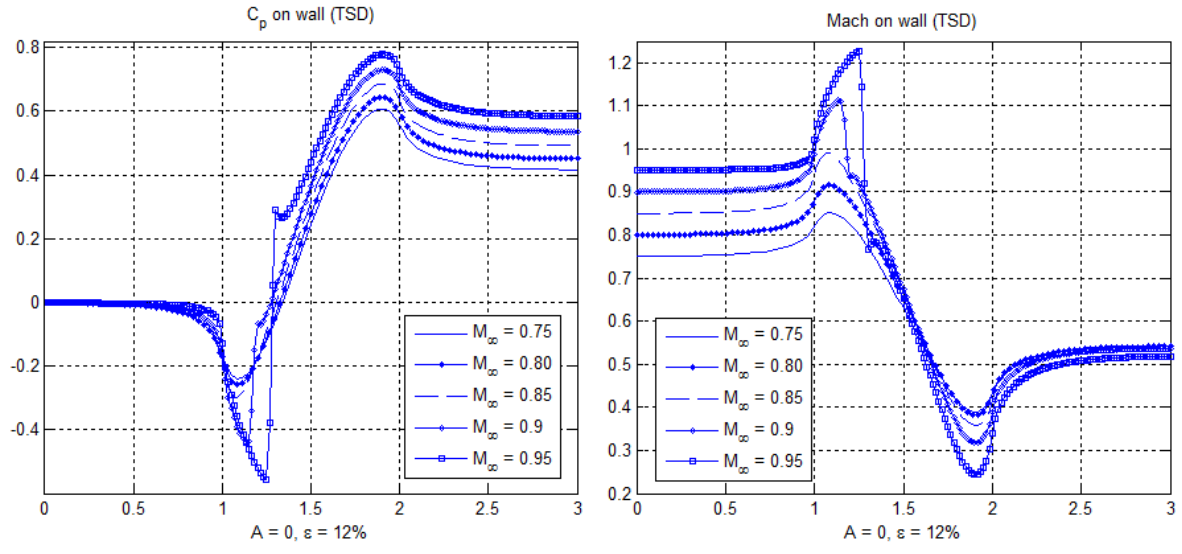

Figure 1: Small Disturbance Model (TSD) for $M_a = 0.75, 0.80, 0.85, 0.90, 0.95$ for A $= 0$, showing transition to shocked flow with Zeirup Singularity at 12% nozzle area variation parameter.

As reported in [8], it is found that higher pre-exponential frequency factor A consumes more reactant and results in a lower thermal energy and higher Mach number at the outlet, see Figure 2. Higher peak Mach number as the duct is widening is also associated in this case with higher A and higher reactant consumption.

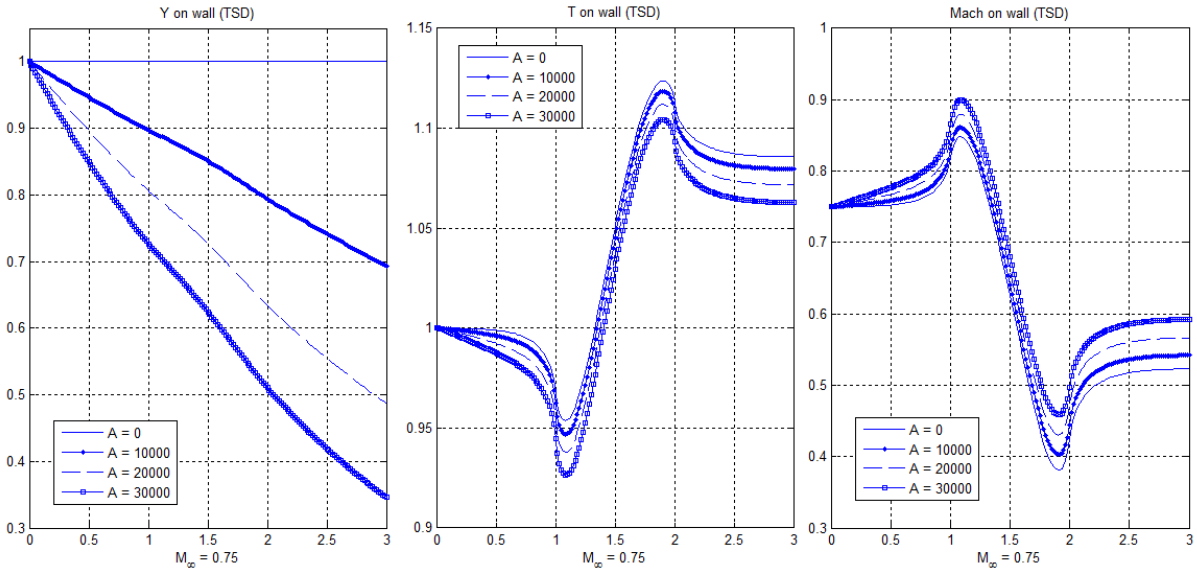

Figure 2: Small Disturbance Model (TSD) T and Y profiles for $M_a = 0.75$ for $A = 0,\ 10000,\ 20000,\ 30000$. Higher pre-exponential frequency factor A consumes more reactant (left), results in a lower thermal energy (middle) and higher Mach number (right) at the outlet.

Similarly, it is found that variation of the channel curvature through the factor ϵ consumes

slightly more reactant and results in a higher thermal energy and lower Mach number at the outlet, see Figure 3.

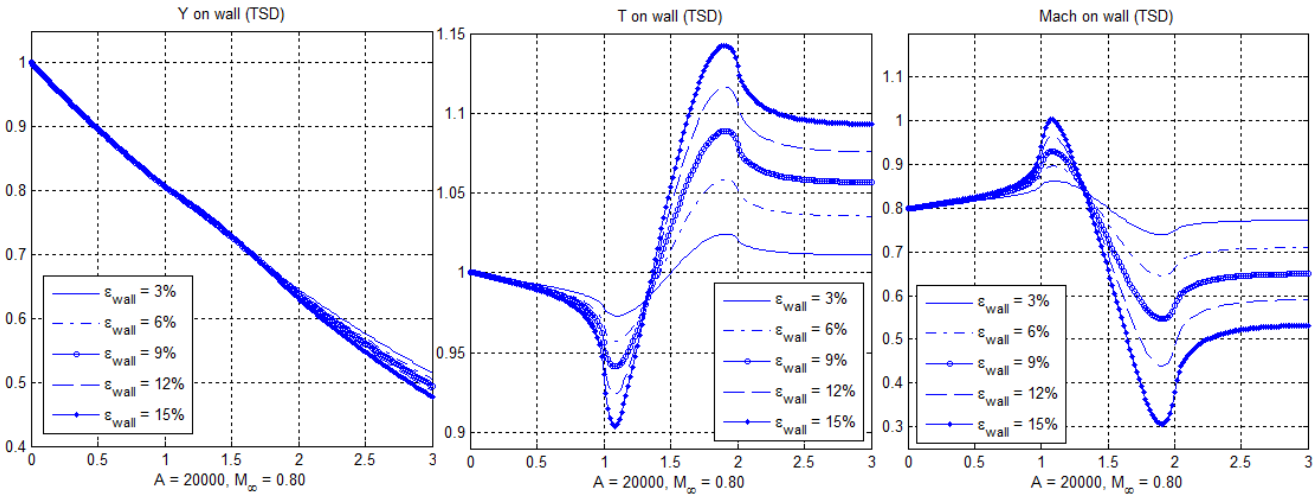

Figure 3: Small Disturbance Model (TSD) T and Y profiles for $M_a = 0.80$, $A = 20000$ for range of channel divergence parameters $\epsilon_{wall} = 3\%, 6\%, 9\%, 12\%, 15\%$. Higher channel divergence consumes more reactant (left) and results in a higher thermal energy (middle) and lower Mach number (right) at the outlet.

An important consequence of the heat release due to combustion is the capability to cause shocks as shown in Figure 4. In this figure, for $M_a = 0.85$, without chemical reaction ($A = 0$) the flow is completely subsonic and smooth, and with chemical reaction ($A = 20000$) the flow contains a supersonic bubble which abruptly becomes subsonic through a normal shock. The outlet Mach number is higher and the outlet coefficient of pressure (C_p) is lower for the reactive flow case where heat is released.

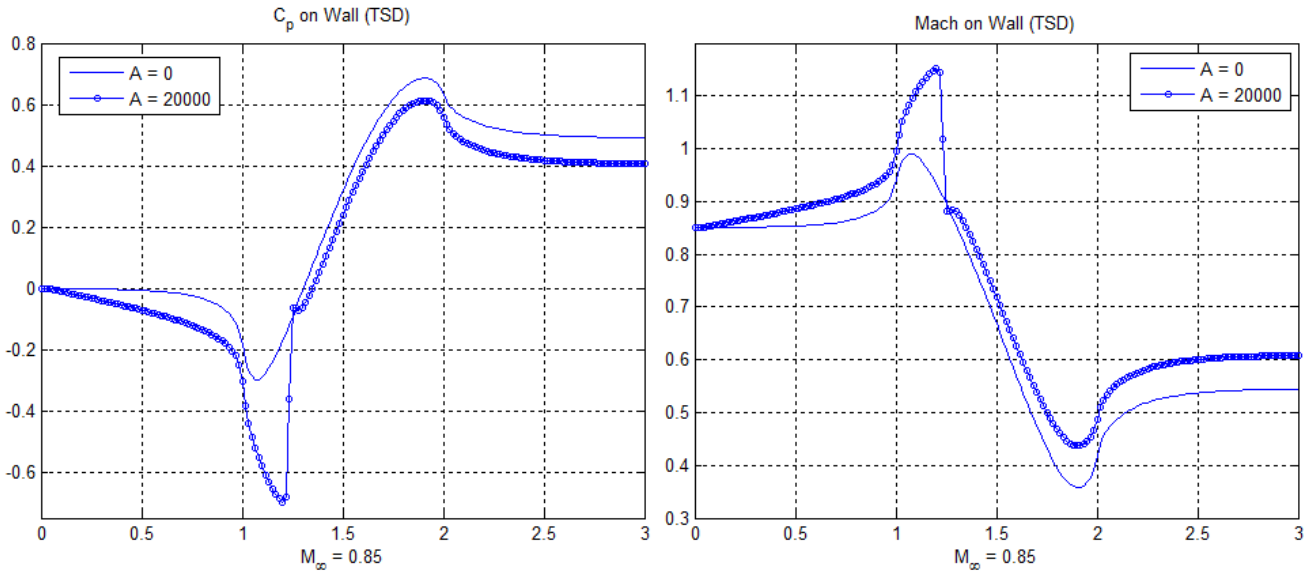

Figure 4: Small Disturbance Model (TSD), $M_a = 0.85$, $A = 0$ and $A = 20000$, shows supersonic bubble due to chemical reaction and small Zierup Singularity.

5 Numerical Methods for the Full Potential Model

To solve the full potential equation we use the artificial compressibility methods [3],[10]. We consider the density biasing and flux biasing formulations.

$$(\rho\phi_x)_x + (\rho\phi_y)_y = 0 \longrightarrow (\bar{\rho}\phi_x)_x + (\bar{\rho}\phi_y)_y = 0 \tag{19}$$

A modified artificial density method that is based on flux biasing is given by:

$$\bar{\rho}_{(i+1/2,j+1/2)} = \rho_{(i+1/2,j+1/2)} - \left[\frac{u}{q^2}\Delta x\frac{\partial F}{\partial x} + \frac{v}{q^2}\Delta y\frac{\partial F}{\partial y}\right]_{(i+1/2,j+1/2)} \tag{20}$$

After calculating the local Mach number at the cell centers:

$$M^2_{(i+1/2,j+1/2)} = \frac{q^2}{a^2} = \frac{u^2+v^2}{\frac{1}{M^2_\infty} + \frac{1}{2}(\gamma-1)\left[1-u^2-v^2\right]} \tag{21}$$

The flux F is calculated at the cell-centers from:

$$F = \begin{cases} \rho q, & \text{for } M > 1 \\ \rho^* q^* = \rho^* a^*, & \text{for } M \le 1 \end{cases} \tag{22}$$

Where the following definitions are used:

$$a^* = \left(2\frac{\gamma-1}{\gamma+1}\left[\frac{1}{\gamma-1}\frac{1}{M^2_\infty} + \frac{1}{2}\right]\right)^{1/2} \tag{23}$$

$$\rho^* = \left(1 - \frac{M^2_\infty(\gamma-1)}{2}((a^*)^2-1)\right)^{1/(\gamma-1)} \tag{24}$$

In the density biasing scheme, instead of biasing the flux $F := \rho q$, now the density alone is biased:

$$\rho_{i+1/2,j+1/2} = \rho_{i+1/2,j+1/2} - \mu \left(\rho_{i+1/2,j+1/2} - \rho_{i-1/2,j+1/2} \right) \tag{25}$$

Where the upwind shifting parameter μ is defined in terms of the local Mach number [4]:

$$\mu = \tau \cdot \max \left(0, 1 - \frac{M_c^2}{M_{i+1/2,j+1/2}^2}, 1 - \frac{M_c^2}{M_{i-1/2,j+1/2}^2} \right) \tag{26}$$

Where τ, M_c^2 are user specified parameters. The energy and species equations are solved using a conservative mixed upwind/centered scheme with backward difference in the x-direction. A staggered grid is used as show in Figure 5:

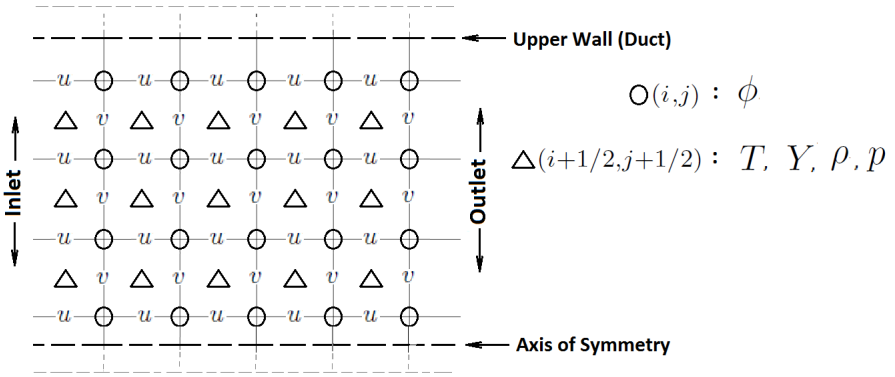

Figure 5: Staggered grid showing the location of the duct, centerline and model variables.

For the case of steady state computations, all the time dependent terms are removed from the governing equations. The pressure Poisson equation is solved for p:

$$-\left[(\rho u^2)_x + (\rho uv)_y\right]_x - \left[(\rho uv)_x + (\rho v^2)_y\right]_y = (p_{xx} + p_{yy}) \tag{27}$$

And the density is updated via the perfect gas law by line successive under relaxation until convergence, where n denotes the iteration count:

$$\rho^{n+1} = \rho^n + \omega_{SOR} \left(\frac{p}{T} \frac{\gamma}{\gamma - 1} - \rho^n \right) \tag{28}$$

Since the the pressure, temperature and species equations are elliptic, they are iteratively solved until convergence before updating the potential function Φ again, and then recalculating the velocity field. For the case of unsteady computations a stability term of the form: $\nu \rho_t$, with $0 < \nu << 1$, is added to the pressure equation to help with convergence:

$$\left[(\rho u^2)_x + (\rho uv)_y\right]_x + \left[(\rho uv)_x + (\rho v^2)_y\right]_y = \rho_{tt} + \nu \rho_t - (p_{xx} + p_{yy}) \tag{29}$$

This term is a natural choice because when small viscosity is present in the momentum equations:

$$\nu\Delta\left[(\rho u)_x + (\rho v)_y\right] \approx -\nu\rho_t \tag{30}$$

Where $0 \leq \nu \leq 1$. One way to proceed is that the pressure equation is solved for ρ and the gas law is used to update p. The other, which has the advantage of being able to treat operators implicitly, is to solve the pressure equation for p and update the density from the gas law. In this case, one must first update the temperature to the current $(n+1)$ time step, T^{n+1}, then, using the gas law, p^{n+1} is solved according to the nonhomogeneous wave equation:

$$\frac{\gamma}{\gamma-1}\left[\frac{\left(\frac{P}{T}\right)^{n+1} - 2\left(\frac{P}{T}\right)^{n} + \left(\frac{P}{T}\right)^{n-1}}{\Delta t^2} + \nu\frac{\left(\frac{P}{T}\right)^{n+1} - \left(\frac{P}{T}\right)^{n-1}}{2\Delta t}\right] - (p_{xx} + p_{yy})^{n+1} = f_x^n + g_y^n \tag{31}$$

Natural boundary conditions from the momentum equations must be used to eliminate spurious solutions.

6 1D Euler vs. 1D Unsteady Full Potential

A validation test case is performed in 1D and compared against the quasi-1D Euler equations following the example given in [1]. We write the energy equation in terms of temperature using the relation:

$$E = \frac{T}{\gamma} + \frac{1}{2}u^2 \tag{32}$$

Then the energy equation becomes:

$$\begin{aligned} (A\rho E)_t + (A\rho u H)_x &= 0 \\ \left(A\rho\left(\frac{T}{\gamma} + \frac{1}{2}u^2\right)\right)_t + \left(A\rho u\left(T + \frac{1}{2}u^2\right)\right)_x &= \epsilon(A\rho E)_{xx} \\ (A\rho T)_t + \frac{\gamma}{2}\left(\frac{(A\rho u)^2}{A\rho}\right)_t + \gamma\left(A\rho u\left(T + \frac{1}{2}u^2\right)\right)_x &= \gamma\epsilon(A\rho E)_{xx} \end{aligned} \tag{33}$$

Differentiation of conservation of mass with respect to t and conservation of momentum with respect to x, inclusive of artificial viscosity terms, gives:

$$\begin{aligned} -(A\rho)_{tt} &= (A\rho u)_{xt} - \epsilon(A\rho)_{xxt} \\ (Ap)_{xx} &= -(A\rho u)_{tx} - (A\rho u^2)_{xx} + (A_x p)_x + \epsilon(A\rho u)_{xxx} \end{aligned} \tag{34}$$

Adding these equations together implies:

$$(Ap)_{xx} - (A\rho)_{tt} = -(A\rho u^2)_{xx} + (A_x p)_x - \epsilon(A\rho)_{xxt} + \epsilon(A\rho u)_{xxx}$$

Therefore, the present pressure based model for the quasi-1D Euler Equations and small artificial viscosity (with strength ϵ) is given by:

$$\begin{aligned}
(A\rho)_{tt} &= (Ap)_{xx} + \left(A\rho u^2\right)_{xx} - \left(\frac{A_x p}{\rho}\right)_x + \epsilon(A\rho)_{xxt} - \epsilon(A\rho u)_{xxx} \\
(A\rho u)_x &= -(A\rho)_t + \epsilon((A\rho u)_{xx} + (A\rho)_{xx}) \\
(Ap)_t &= -\frac{\gamma-1}{2}\left(A\rho u^2\right)_t - (\gamma-1)\left(A\rho u\left(T + \frac{1}{2}u^2\right)\right)_x (\gamma-1)\epsilon(Ap)_{xx} \\
T &= \frac{\gamma}{\gamma-1}\frac{p}{\rho}
\end{aligned} \tag{35}$$

This system is hyperbolic and converges with $\Delta t = O(\Delta x)$. Alternatively, one can solve the continuity equation for a potential function ϕ, where $u = \phi_x$, without loss of generality as is proposed in the present model.

$$(A\rho\phi_x)_x + (A\rho)_t = 0 \tag{36}$$

A comparison showing the quasi-1D Euler equations (left) and the quasi-1D full potential model (right) is shown in Figure 6. The correct shock location ($x = 0.82$) and flow through the sonic point is acheived in both models.

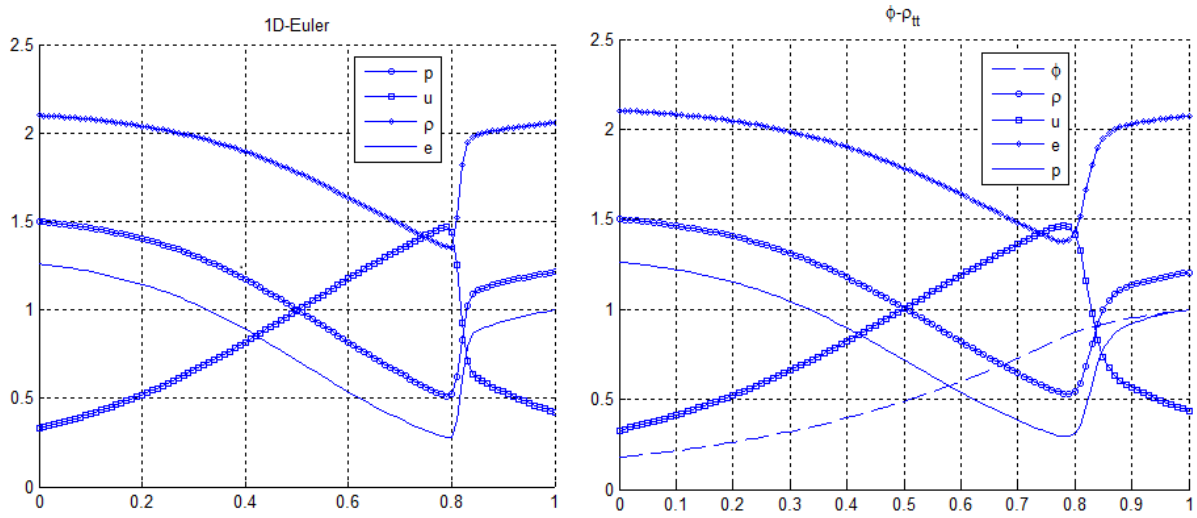

Figure 6: Compressible Nozzle Flow 1D Validation Test Case. Quasi-1D Euler equations (left) and the quasi-1D full potential model (right)

7 Results of the Present Two-Dimensional Full Potential Model

The small disturbance model is essentially mixed type in the x-direction only. In contrast, the full potential can handle mixed type flows in multiple principal directions. As in the small disturbance model, a validation case showing the transition from fully subsonic to shocked flow with a supersonic bubble for a non-reactive flow case is shown first in Figure 7.

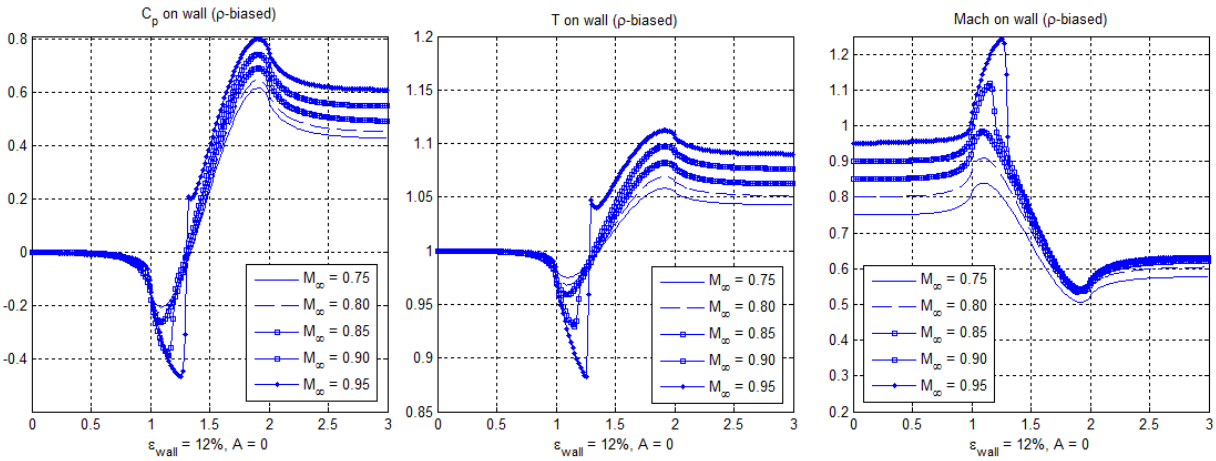

Figure 7: ρ-biased full potential model for $M_a = 0.75, 0.80, 0.85, 0.90, 0.95$ for A $= 0$, showing transition to shocked flow at 12% nozzle area variation parameter.

When the full scheme is used, the results are slightly different from the small disturbance model, although the shock location prediction as well as peak Mach numbers are similar. The pre-shock solution and shock location are very similar, the post shock conditions are seen to vary between the TSD and full potential model, as shown in Figure 8.

The profiles for Y and T are markedly different from the TSD model. In particular, where the TSD model predicts that temperature trends like C_p, in the full model, the temperature increases with heat release. The Y profiles are similar to that of the TSD model, but in our calculations there is a more noticeable effect of the geometry creating variation in reactant consumption rate.

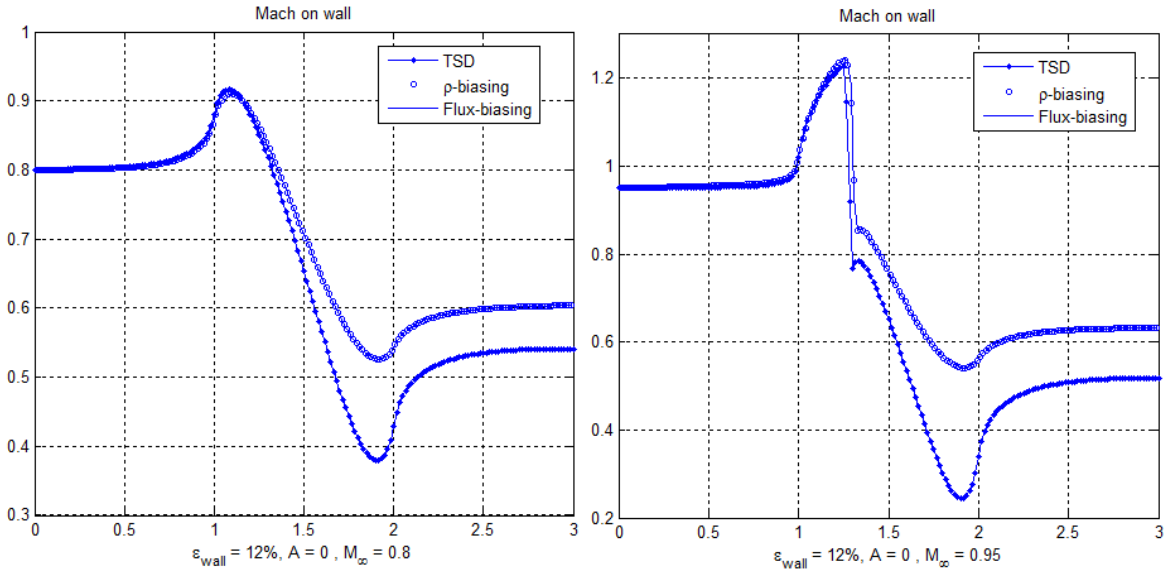

Figure 8: Flux Biasing and ρ-Biasing vs. TSD with $A = 0$ for $M_a = 0.8$ (left) and for $M_a = 0.95$ (right).

In Figure 9 the case of $M_\infty = 0.8$ for a range of pre-exponential frequency factors $A = 0,\ 10000,\ 20000,\ 30000$ is computed. This result is in good agreement with the small disturbance model.

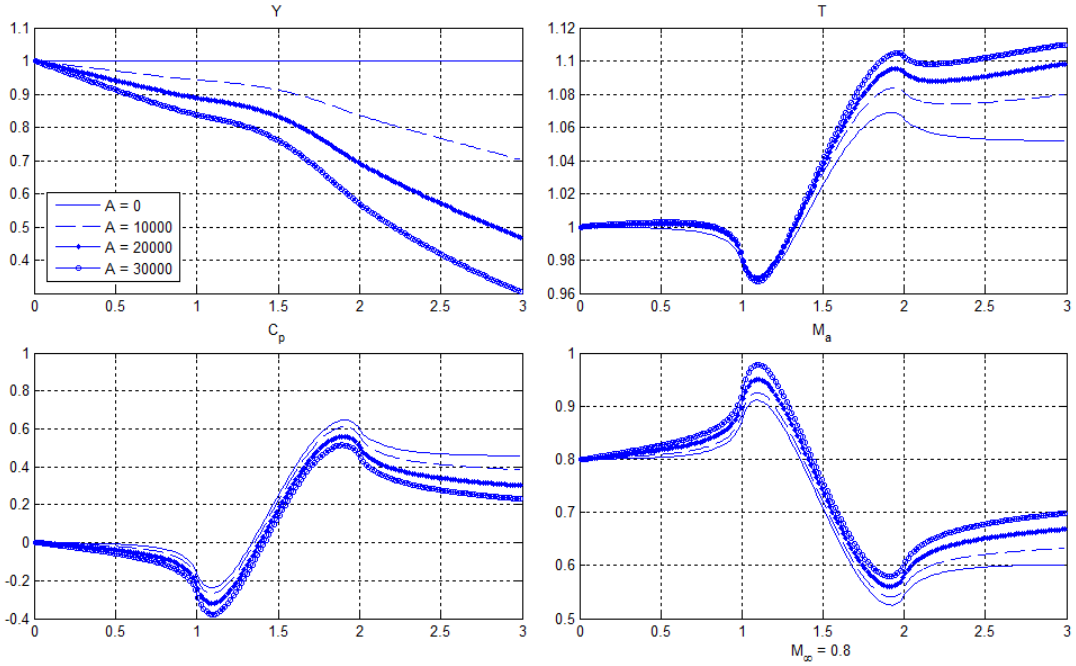

Figure 9: ρ-biased full potential model with $M_\infty = 0.8$ for $A = 0,\ 10000,\ 20000,\ 30000$.

In Figure 10 the case of $M_\infty = 0.85$ for a range of pre-exponential frequency factors $A = 0,\ 10000,\ 20000,\ 30000$ is computed. In this case, the results show the combustion induces a supersonic flow bubble. The trend with respect to Mach number and pressure coefficient are in agreement with the small disturbance model. As in the case with the TSD model, without chemical reaction ($A = 0$) the flow is completely subsonic and smooth, and with chemical reaction a supersonic bubble is shown to develop, the outlet Mach number is higher and the outlet coefficient of pressure (C_p) is lower for the reactive flow cases where heat is released.

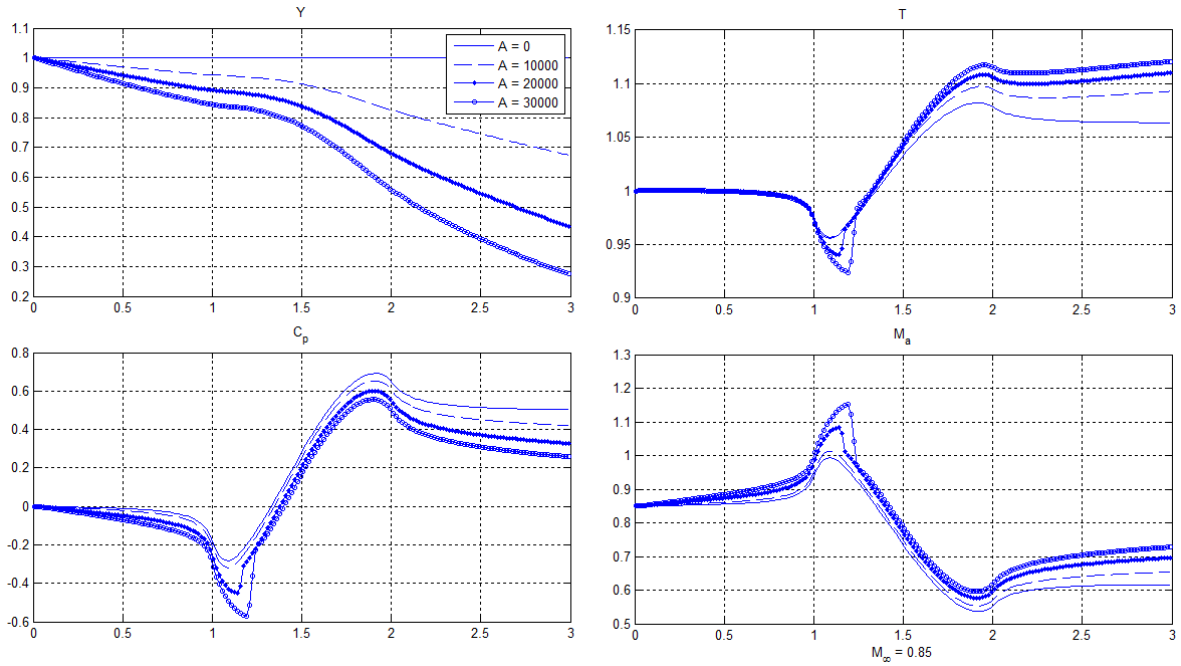

Figure 10: ρ-biased full potential model with $M_\infty = 0.85$ for $A = 0, 10000, 20000, 30000$.

In Figure 11 the case of incident ρ-biased full potential model for $M_\infty = 0.80, 0.85, 0.90, 0.95$ with $A = 20000$ is computed.

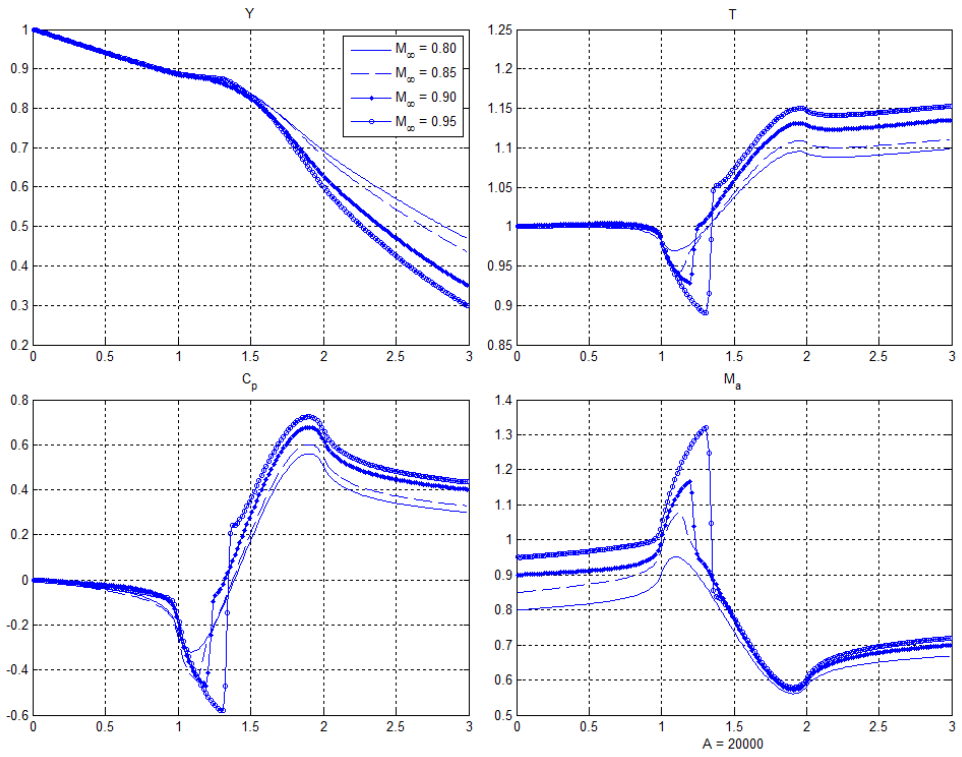

Figure 11: ρ-biased full potential model for $M_\infty = 0.80, 0.85, 0.90, 0.95$ with $A = 20000$.

An unsteady example has been computed as a validation test for $M_\infty = 0.80$ with $A = 0$. The results are in good agreement with the steady state model and are shown in Figure 12.

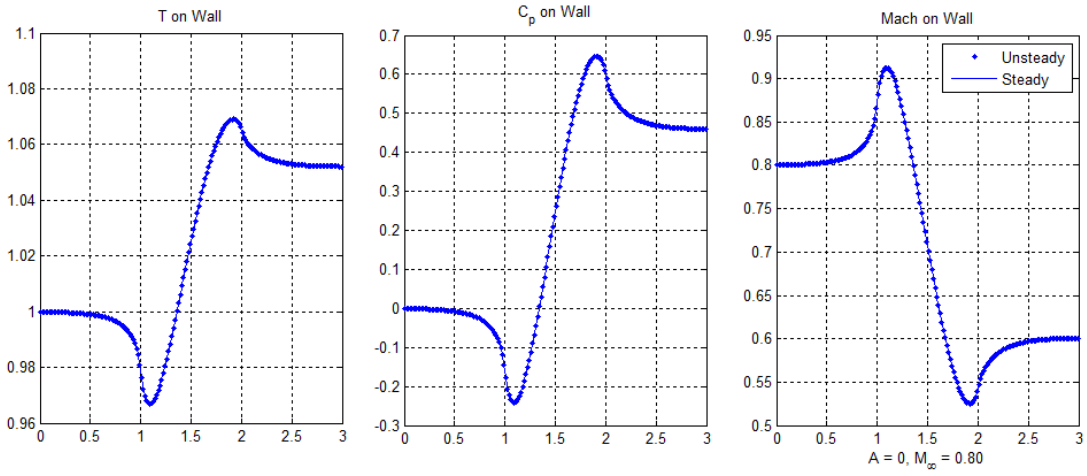

Figure 12: ρ-biased unsteady full potential model for $M_\infty = 0.80$ with $A = 0$ validating the unsteady model converges to the same steady state solution.

Also the case where combustion causes a shock in the flow for $M_\infty = 0.85$ with $A = 20000$ has

been computed. The results are shown in Figure 13 and indicates the unsteady model produces a slightly sharper shock that is in nearly the same location as the steady model.

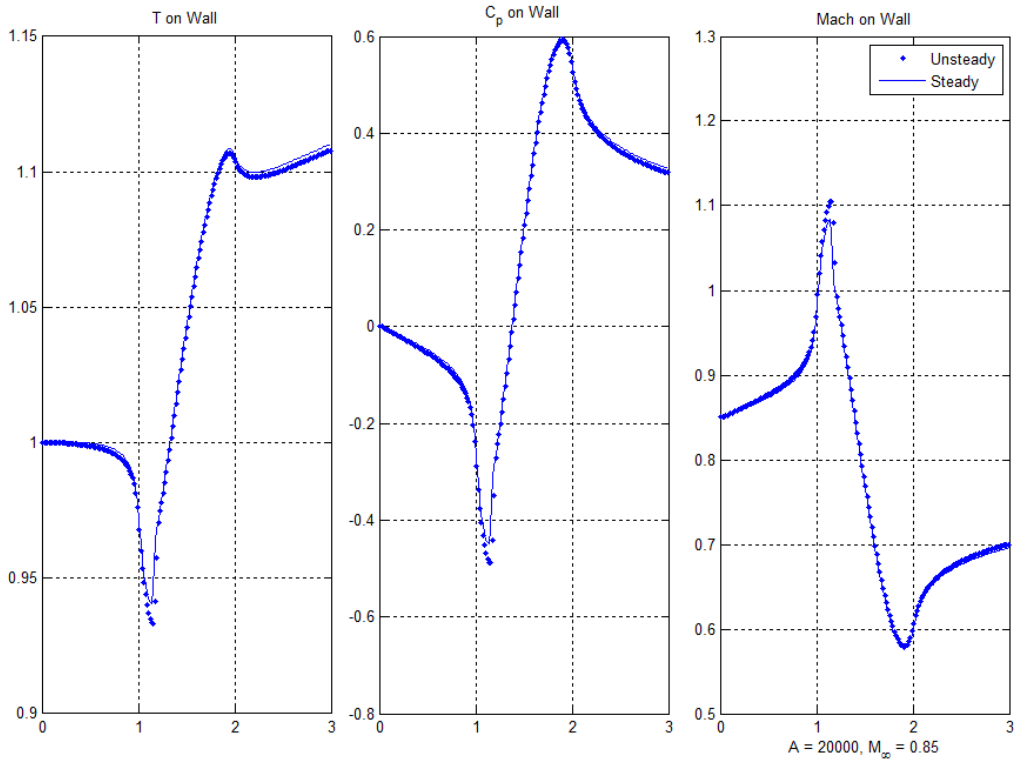

Figure 13: ρ-biased unsteady full potential model for $M_\infty = 0.85$ with $A = 20000$ showing the steady state and unsteady solution overlayed

The time dependent transient history for $M_\infty = 0.85$ with $A = 20000$, starting from uniform quiescent initial data show the effect of combustion on the peak Mach number and fuel consumption in Figure 14. This result shows that the steady state exists and that startup can cause shocked flow, but the long time behavior of the solution is not dependent on this transient behavior.

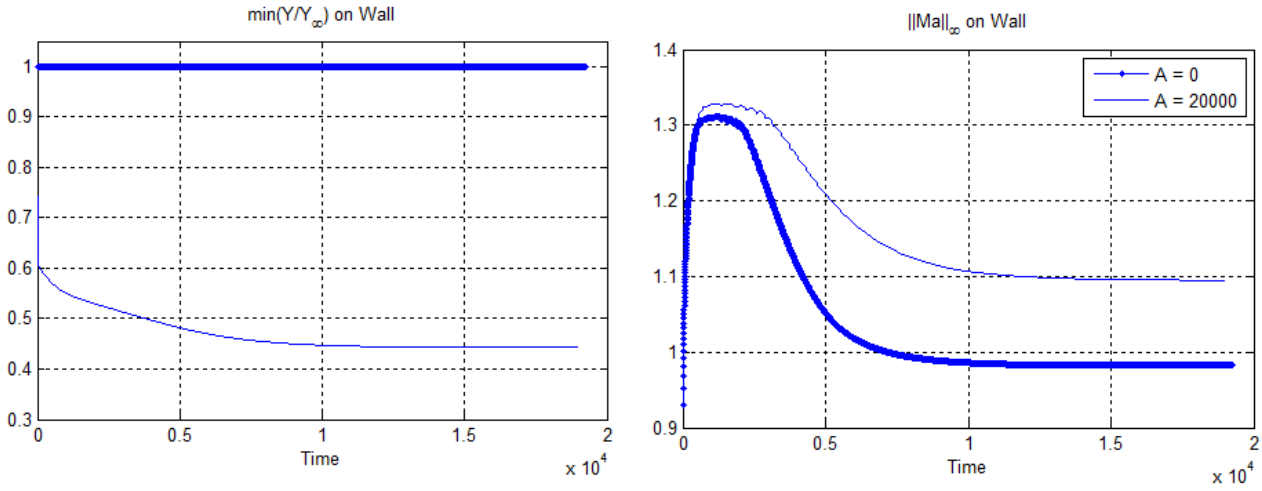

Figure 14: Unsteady peak Mach number (right) and minimum Y value (left) along the wall for $M_\infty = 0.85$ with $A = 0, 20000$. It is shown that the unsteady code converges from quiescent initial conditions to the same solution as the steady code.

8 Conclusions

It is clear that the small disturbance approach is limited to small heat release and small area variation. Although the small disturbance model is limited in its range of applicability, within that range it can be fast to apply and may produce quite reasonable results. The full potential model is more general and should be able to handle a larger heat release and area variation. In addition, it should be straightforward to include a more detailed reaction mechanism without significant modifications to the model.

REFERENCES

[1] Chattot, J.J. *Computational Aerodynamics and Fluid Dynamics.* Springer-Verlag Berlin Heidelberg New York, 2002.

[2] Cole, J. D., Cook, L. P. *Transonic Aerodynamics.* Elsevier Science Publishers B.V (1986)

[3] Hafez, M.M., South, J. and Murman, E.M. *Artificial Compressibility Methods For Numerical Solution of Transonic Full Potential Equation.* AIAA Journal, Vol. 17, No. 8:838-844 (1979)

[4] Hafez, M.M., Habashi, W.G., Kotiuga, P.L. *Conservative calculations of non-isentropic transonic flows.* International Journal for Numerical Methods in Fluids, Vol 5: 1047-1057 (1985)

[5] Holst, T.L. *Numerical Computation of Transonic FLow Governed by the Full-Potential Equation.* (N83-19708) NASA Technical Memorandum 84310 (1983)

[6] Murman. E. M. and Cole. J. D. *Calculation of Plane Steady Transonic flow* AIAA S., Vol. 9. No. 1, pp 114-121 (1971)

[7] Osher, S., Hafez, M., Whitlow, Jr., W. *Entropy Condition Satisfying Approximations for the Full Potential Equation of Transonic Flow* Mathematics of Computation, Vol. 44, No.

169:1-29 (1985)

[8] Rusak, Z; Lee, J.C; Choi, J.J. *A small-disturbance model of transonic combustion.* Combustion Theory and Modeling, 12: 1, p. 93-113 (2007)

[9] Rusak, Z; Lee, J.C. *Parametric Investigation of Combustion in Compressible Flows.* AIAA-2005-4805: 4th AIAA Theoretical Fluid Mechanics Meeting, (2005)

[10] Volpe, G., Jameson, A. *Transonic Potential Flow Calculations by Two Artificial Density Methods.* AIAA Journal, Vol. 26, No. 4, (1988)